Biochem. J. (2013) **450**, 477–486 (Printed in Great Britain) doi:10.1042/BJ20121305

online data

Allosteric inhibition of VIM metallo-β-lactamases by a camelid nanobody

Jean S. SOHIER*, Clémentine LAURENT*, Andy CHEVIGNÉ†, Els PARDON‡§, Vasundara SRINIVASAN‡§, Ulrich WERNERY‖, Patricia LASSAUX*, Jan STEYAERT‡§ and Moreno GALLENI*[1]

*Centre for Protein Engineering, Macromolecules Biologiques Unit, University of Liège, Allée du 6 Août, 13 (B6A), Sart-Tilman, 4000 Liege, Belgium, †Public Research Centre for Health (CRP-Santé), Laboratory of Retrovirology, Val Fleuri 84, L-1526 Luxembourg, Luxembourg, ‡Department of Structural Biology (VIB), Pleinlaan 2, 1050 Brussels, Belgium, §Structural Biology Brussels, Vrije Universiteit Brussel, Pleinlaan 2, 1050 Brussels, Belgium, and ‖Central Veterinary Research Laboratory, P.O. Box 597, Dubai, United Arab Emirates

MβL (metallo-β-lactamase) enzymes are usually produced by multi-resistant Gram-negative bacterial strains and have spread worldwide. An approach on the basis of phage display was used to select single-domain antibody fragments (V_HHs, also called nanobodies) that would inhibit the clinically relevant VIM (Verona integron-encoded MβL)-4 MβL. Out of more than 50 selected nanobodies, only the NbVIM_38 nanobody inhibited VIM-4. The paratope, inhibition mechanism and epitope of the NbVIM_38 nanobody were then characterized. An alanine scan of the NbVIM_38 paratope showed that its binding was driven by hydrophobic amino acids. The inhibitory concentration was in the micromolar range for all β-lactams tested. In addition, the inhibition was found to follow a mixed hyperbolic profile with a predominantly uncompetitive component. Moreover, substrate inhibition was recorded only after nanobody binding. These kinetic data are indicative of a binding site that is distant from the active site. This finding was confirmed by epitope mapping analysis that was performed using peptides, and which identified two stretches of amino acids in the L6 loop and at the end of the α2 helix. Because this binding site is distant from the active site and alters both the substrate binding and catalytic properties of VIM-4, this nanobody can be considered as an allosteric inhibitor.

Key words: allosteric inhbition, metallo-β-lactamase, nanobody.

INTRODUCTION

The production of β-lactamases represents the most prevalent bacterial-resistance mechanism against β-lactam antibiotics. These enzymes catalyse the cleavage of the amide bond of the β-lactam ring to inactivate the antibiotic. On the basis of sequence identity, β-lactamases have been grouped into four molecular classes [1]. Among them, the class B MβLs (metallo-β-lactamases) are zinc-dependent enzymes that display a characteristic H(N/Q)^{116}XH^{118}XD^{120} motif (class B β-lactamase standard numbering scheme [2]) and a symmetrical $\alpha\beta/\beta\alpha$ fold that probably results from an ancestral gene duplication event [3,4].

MβLs are characterized by their efficient hydrolysis of 'last resort' β-lactam carbapenems; however, MβLs also hydrolyse a broad spectrum of clinically useful β-lactam antibiotics, with the exception of monobactams. Despite their generally low degree of similarity, MβL coding sequences are divided into three structural subclasses (B1, B2 and B3) on the basis of differences in amino acid residues that co-ordinate Zn^{2+} at positions 116 and 221 [5]. In addition to chromosomally encoded MβLs, such as BcII (B1 from *Bacillus cereus*), CphA (B2 from *Aeromonas hydrophila*) or L1 (B3 from *Stenotrophomonas maltophilia*), most of the acquired MβLs such as IMP (imipenemase), VIM (Verona integron-encoded MβL), GIM (German imipenemase), SPM (Sao Paolo MβL) or NDM (New Delhi MβL) types belong to the subclass B1 and are mainly encountered in *Pseudomonas aeruginosa*, *Acinetobacter baumannii* and Enterobacteriaceae isolates [6]. The rapid spread of acquired B1 MβLs now represents a worldwide threat to healthcare [7,8].

B1 MβLs are able to bind up to two metal ions, Zn1 and Zn2, which are located in two different co-ordinating sites that are often referred to as the 3H and DCH sites respectively. These enzymes are active in their mononuclear and dinuclear forms *in vitro*, but exhibit their maximal activities as di-zinc species [9]. The B1 MβL active site is located in a groove between the two $\alpha\beta$ domains and is essentially composed of loops (Figure 1) [10]. Four loops are involved in the co-ordination of the two Zn^{2+} ions through His^{116}, His^{118} and Asp^{120} (these three amino acids are on loop L7), His^{196} (on loop L9), Cys^{221} (on loop L10) and His^{263} (on loop L12). These four loops define the floor of the active site, whereas loop L3 (the so-called flapping loop) and the main part of loop L10 are exposed on each $\alpha\beta$ domain and flank the active site. The selection of broad-spectrum inhibitors against MβLs is hampered by the diversity of MβLs, their mechanisms that do not involve any highly populated metastable reaction intermediates, and the fact that the compound must remain inactive towards similar human proteins. To date, all of the compounds that have been tested have failed to meet all of these criteria for successful medical application [11–13].

Therefore we wanted to pursue the approach initiated by Conrath et al. [14], who identified a camelid single-domain antibody fragment that inhibits the BcII MβL. Camelid immune systems produce HcAbs (heavy-chain homodimer antibodies) that are devoid of light chains; therefore the antigen-binding domains of HcAbs consist of a single domain called a nanobody [15]. Owing to their small paratopes, nanobodies are able to recognize epitopes that are not accessible to conventional antibodies, such as clefts and cavities in the enzyme active site [16]. Various enzymes have been inhibited by selected

Abbreviations used: Amp^R, ampicillin-resistance; CDR, complementarity-determining region; cfu, colony-forming units; Chl^R, chloramphenicol-resistance; DTT, dithiothreitol; FR2, framework 2; HcAb, heavy-chain homodimer antibody; HRP, horseradish peroxidase; IMAC, immobilized metal-ion-affinity chromatography; IMGT, International ImMunoGeneTics; IMP, imipenemase; IPTG, isopropyl β-D-thiogalactopyranoside; LB, Luria–Bertani; MβL, metallo-β-lactamase; MD, molecular dynamics; MWCO, molecular-mass cut-off; PBST, 0.05 % Tween 20 in PBS; sulfo-NHS-SS-biotin, sulfosuccinimidyl-2-(biotinamido)ethyl-1,3-dithiopropionate; TB, terrific broth; VIM, Verona integron-encoded MβL; WT, wild-type.

[1] To whom correspondence should be addressed (email mgalleni@ulg.ac.be).

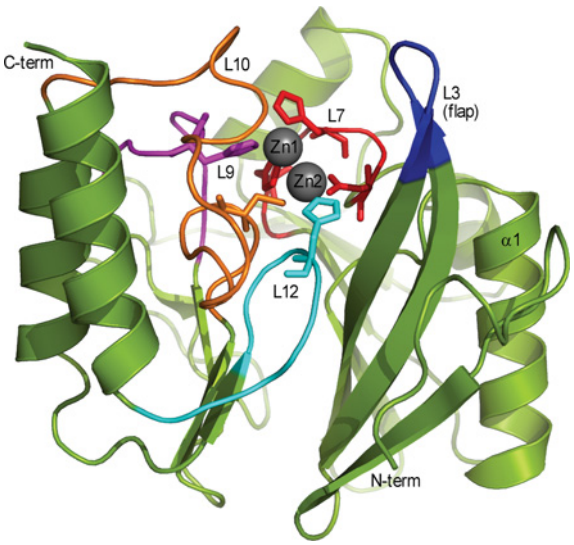

Figure 1 Crystallographic structure of VIM-4 (PDB code 2WHG)

The L3 (flapping loop), L7, L9, L10 and L12 loops are shown in blue, red, magenta, orange and cyan respectively.

nanobodies [17–20]. Two nanobodies that give rise to hyperbolic inhibition profiles have been described as allosteric effectors of the DHFR (dihydrofolate reductase) and *Tv*NH (*Trypanosoma vivax* nucleoside hydrolase) enzymes [21,22]. In the present study, a llama and a dromedary were immunized with VIM-4 to select inhibitory nanobodies. The enzyme VIM-4 was responsible for an outbreak in Greece and has been detected in several coutries worldwide [23]. We performed a steady-state characterization of the VIM-4 inhibition by the isolated NbVIM_38 nanobody and identified its binding site on the surface of VIM-4. Because this epitope is far from the active site, we concluded that the NbVIM_38 nanobody behaves as an allosteric effector.

EXPERIMENTAL

Preparation of VIM-4

The enzyme VIM-4 was produced following the auto-induction strategy as described by Studier [24]. The *Escherichia coli* BL21-CodonPlus(DE3) cells transformed with the expression plasmid pET9a/VIM-4 [25] were grown overnight in 250 ml of MDG medium supplemented with 25 μg/ml chloramphenicol, 10 μg/ml tetracycline and 100 μg/ml kanamycin. This preculture was used to inolulate a 10 litre bioreactor filled with a modified ZYM-5052 medium (1 % tryptone, 0.5 % yeast extract, 25 mM Na_2HPO_4, 25 mM KH_2PO_4, 50 mM NH_4Cl, 5 mM Na_2SO_4, 2 mM $MgSO_4$, 0.2 % α-lactose, 0.05 % glucose, 2 % glycerol and 2× trace metal mix solution). The pH was set to 6.9, and the dissolved oxygen was maintained at 40 % (100 % being the level of dissolved oxygen in the autoclaved fermenter before fermentation). The culture was incubated for 4 h at 37 °C. The temperature was subsequently decreased to 28 °C to initiate the production of β-lactamase. After 25 h of culture, an A_{600} of 25 was obtained, and the cells were recovered using a Westfalia separator (model KA05-00-105). The cells were homogenized in 1 litre of 10 mM Hepes and 50 μM $ZnCl_2$ (pH 7.5) (buffer A) and lysed using a cell disruptor (GEA PANDA 2k). Cellular debris was removed by centrifugation for 30 min at 25 000 ***g***. The crude extract was then divided into smaller batches. Each lysate was first clarified by the progressive addition of 50 % ammonium sulfate at 4 °C. After centrifugation, the supernatant was dialysed against buffer A and applied to a QHP column (60 ml; GE Healthcare). The VIM-4 MβL was eluted using a linear gradient from 0 to 1 M NaCl in buffer A. The VIM-4-containing fractions were pooled, dialysed against buffer A and then further purified using a Source 15Q column (20 ml; GE Healthcare). VIM-4 was eluted with the help of a linear NaCl gradient (0–1 M) in buffer A. The β-lactamase-containing fractions were concentrated by ultrafiltration [10 kDa MWCO (molecular-mass cut-off), Vivaspin] and loaded on to a Superdex S200PG gel-filtration column (490 ml; GE Healthcare) that was previously equilibrated in buffer A. The purity was assessed by SDS/PAGE (15 % gels), and the final protein concentration was determined by using the molar absorption coefficient at 280 nm ($\varepsilon = 28420\ M^{-1} \cdot cm^{-1}$), which was calculated using ProtParam (ExPASy Proteomics Server, http://expasy.org/).

For use during the phage display experiments, the purified VIM-4 enzyme was labelled in PBS using the EZ-Link sulfo-NHS-SS-biotin [sulfosuccinimidyl-2-(biotinamido)ethyl-1,3-dithiopropionate] biotinylation reactant (Pierce) following the manufacturer's instructions. The MβL activity was shown to be preserved after biotinylation.

Phage display

Animal experiments followed the guidelines published by the regional United Arab Emirates government. A llama and a dromedary were immunized six times with the MβL VIM-4 (2 mg in total) to collect lymphocytes whose nanobodies nucleotide sequences were amplified by RT (reverse transcription)–PCR; this procedure has been described previously [14,26]. The PCR fragments were ligated into a pHEN11 phagemid vector containing the Chl^R (chloramphenicol-resistance) gene (referred to as pHEN4C in Conrath et al. [14]) and transformed into *E. coli* TG1 cells.

The VIM-4-specific llama nanobodies were selected on solid-phase coated antigen (see Supplementary Experimental section at http://www.biochemj.org/bj/450/bj4500477add.htm) and in solution using the biotinylated antigen and magnetic streptavidin beads (Dynabeads M280; Invitrogen) [27]. The anti-VIM-4 dromedary nanobodies were only selected using the latter method. Briefly, 3×10^{11} phages were incubated with 100 nM biotinylated VIM-4 in 1 ml of PBS with 1 % BSA for 1 h at room temperature (25 °C) on an end-over-end rotator. Blocked magnetic beads (1 h, 2 % powdered milk) were then added to trap the antigen–phage complexes. The beads were washed ten times with 1 ml of PBST (0.05 % Tween 20 in PBS) using a magnetic separator. The complexes were eluted by resuspending the beads in 200 μl of 50 mM DTT (dithiothreitol) in PBS and incubating the tubes for 15 min on an end-over-end rotator at room temperature. TG1 cells were then infected with eluted phages and streaked out for screening. Only one round of selection was necessary to achieve a sufficient enrichment. The expression of the nanobody binder in randomly chosen colonies was then confirmed, as explained in the Supplementary Experimental section.

Nanobody expression and inhibitor screening

The pHEN14 plasmid is derived from the pHEN6(c) expression vector [24,28], which has been modified by replacing the Amp^R (ampicillin-resistance) AatII/HindIII cassette by the corresponding Chl^R cassette from the phagemid pHEN11. The resulting plasmid also contains the sequences for the pelB signal peptide and a histidine tag. The plasmid was used for the expression

of the recombinant nanobodies in the *E. coli* WK6 strain. Nanobody production was achieved by growing the bacteria in 250 ml of TB (terrific broth) medium supplemented with 25 μg/ml chloramphenicol until an A_{600} of 0.6–0.9 was reached. Expression was induced by the addition of 1 mM IPTG (isopropyl β-D-thiogalactopyranoside) and subsequent incubation for 16 h at 28 °C. After pelleting the cells, the periplasmic proteins were extracted by osmotic shock. The extracts were directly purified using an IMAC (immobilized metal-ion-affinity chromatography) column on a Profinia Platform (Bio-Rad Laboratories) according to the manufacturer's instructions. The purity of the proteins was evaluated by SDS/PAGE, and the final protein concentration was determined using the molar absorption coefficients at 280 nm, which were calculated by ProtParam (ExPASy Proteomics Server, http://expasy.org/).

The inhibition of VIM-4 activity by the purified nanobodies was monitored in microplates by measuring the VIM-4-mediated initial hydrolysis rates of 100 μM nitrocefin at 482 nm ($\Delta\varepsilon = 15000\ M^{-1} \cdot cm^{-1}$) in buffer containing 10 mM Hepes and 50 μM $ZnCl_2$ (pH 7.2) that was supplemented with 0.2 mg/ml BSA and the presence or absence of 5 μM nanobodies. The measurements were recorded using a PowerWaveX microplate reader (Bio-Tek Instruments).

Preparation of cherry–NbVIM_38

The DNA fragment containing the sequence of NbVIM_38 was amplified by PCR in order to add 5′-BamHI and 3′-XhoI restriction sites. The PCR fragment was then subcloned into a pGEM-T Easy cloning vector (Promega) before cloning into a modified pSCherry1 expression vector (Eurogentec) in which the Amp^R gene cassette was replaced by the Kan^R (kanamycin-resistance) selection marker from the pET28a vector. This modified pSCherry1 expression vector allows the cytoplasmic production of a cherry–NbVIM_38 fusion protein with a C-terminal histidine tag.

E. coli BL21(DE3) cells transformed with the expression vector were grown at 37 °C in 2 litres of LB (Luria–Bertani) medium supplemented with 50 μg/ml kanamycin until an A_{600} of 0.5–0.8 was reached. The expression of the nanobody was induced by adding 1 mM IPTG. The culture was then incubated for 18 h at 18 °C. The cells were recovered by centrifugation at 10500 ***g*** for 20 min, resuspended in 100 ml of PBS and lysed using an EmulsiFlex-C3 cell disrupter (Avestin). The cytoplasmic extract was clarified by centrifugation for 15 min at 4 °C at 38000 ***g***. The soluble fraction was loaded on to a 12 ml Ni^{2+}-PDC Streamline IMAC affinity column that was equilibrated in PBS. The bound proteins were eluted over a 120 ml linear imidazole gradient (0–250 mM) in PBS. The fractions containing the cherry–NbVIM_38 protein were concentrated by ultrafiltration (10 kDa MWCO, Vivaspin) and loaded on to a 490 ml Superdex S200PG gel-filtration column that was equilibrated in 10 mM Hepes and 100 mM NaCl (pH 7.2). The purity was assessed by SDS/PAGE (15 % gels), and the final protein concentration was determined using the molar absorption coefficient ($\varepsilon_{280} = 36120\ M^{-1} \cdot cm^{-1}$).

Alanine scanning

Alanine-scanning mutagenesis of the residues in the CDR2 and CDR3 (CDR is complementarity-determining region) regions was performed following the general procedure of the QuikChange® site-directed mutagenesis kit (Stratagene). The pGEM-T Easy vector (Promega) containing the BamHI-XhoI NbVIM_38 coding sequence was used as a template for the amplification of the mutated NbVIM_38 coding sequences using the Platinum Pfx polymerase (Invitrogen). The primers used in the present study are listed in Supplementary Table S1 (at http://www.biochemj.org/bj/450/bj4500477add.htm). The BamHI-XhoI inserts were then ligated into the modified pSCherry1 expression vector.

All mutant nanobodies were produced as described above for the WT (wild-type) cherry-fusion protein in 250 ml of LB medium. Soluble fractions containing mutated proteins were purified by IMAC in phosphate buffer on a Profinia platform (Bio-Rad Laboratories). The 18 purified cherry–nanobody solutions were normalized to a final concentration of 35 μM in 10 mM Hepes buffer (pH 7.4).

The inhibitory properties of the different nanobody mutants were determined as described above. The residual activities were measured in triplicate and expressed as inhibition percentages.

Epitope mapping

The scanning peptide array that displayed 112 overlapping dodecapeptides (offset two amino acids), which cover the entire sequence of VIM-4, was designed using Intavis MultiPep software. It was constructed in triplicate on a PEG [poly(ethylene glycol)]-derivatized cellulose membrane (Proteigene) using an AutoSpot SL semi-automated robot (Intavis AG). Three scrambled peptides were also introduced as negative controls. The peptides were synthesized on to the membrane in a stepwise manner starting at the attached C-terminus and ending at the exposed N-terminus, as explained in the Supplementary Experimental section. The peptides recognized upon addition of 5 μM cherry–NbVIM_38 were visualized by immunodetection using the anti-HIS6 HRP (horseradish peroxidase)-conjugated antibody (Roche Applied Science) according to the manufacturer's instructions.

An additional ELISA experiment was performed with biotinylated dodecapeptides (offset four amino acids, Biotides, JPTPeptide Technology), covering the epitope previously identified on the peptide array. Peptide dilutions were immobilized on Nunc Immobilizer streptavidin plates (Thermo Scientific). After washing with PBST, 5 μM cherry–NbVIM_38 in PBST/0.1 % BSA was incubated for 1 h at room temperature. The anti-HIS6 HRP-conjugated antibody (Roche Applied Science) was used in combination with the TMB (3,3′,5,5′-tetramethylbenzidine) substrate (Sigma) to detect peptides recognized by cherry–NbVIM_38. The absorbances at 450 nm were normalized for the total signal.

Kinetic characterization

Increasing amounts of cherry–NbVIM_38 (0–8 μM) were mixed with 0.2 nM VIM-4 in a buffer containing 10 mM Hepes and 20 μM $ZnCl_2$ (pH 7.2) supplemented with 0.2 mg/ml BSA. Cephalothin, a reporter substrate, was then added at final concentrations ranging from 5 to 90 μM. The initial rate of hydrolysis was monitored at 273 nm ($\Delta\varepsilon = -6300\ M^{-1} \cdot cm^{-1}$) using a Specord 200 spectrophotometer (Analytik Jena) equipped with a six-cell changer. The reactions were performed in duplicate at 30 °C. A global non-linear curve fitting of the initial velocities was performed using the GraphPad Prism 5.04 software. Eqn (1), which corresponds to Scheme 1, was used; the k_{cat}, K_m, K_i, K_{si}, α and β parameters in eqn (1) were constrained in the analysis to be shared in all datasets.

Table 1 Steady-state parameters of VIM-4 purified from cultures made with different contents of Zn^{2+}

$-[Zn^{2+}]$ refers to 2 μM $ZnSO_4$ in the ZYM-5052 culture medium (0.2× trace metal solution) [24]. $+[Zn^{2+}]$ refers to 20 μM $ZnSO_4$ in the ZYM-5052 culture medium (2× trace metal solution) [24]. The individual kinetic parameters are the means of three measurements that were obtained with the addition of 20 μM $ZnCl_2$. The S.D. values were below 10 % in all cases.

	k_{cat} (s^{-1})		K_m (μM)		k_{cat}/K_m ($\times 10^6$) ($M^{-1} \cdot s^{-1}$)	
Substrates	$-[Zn^{2+}]$	$+[Zn^{2+}]$	$-[Zn^{2+}]$	$+[Zn^{2+}]$	$-[Zn^{2+}]$	$+[Zn^{2+}]$
Benzylpenicillin	97	650	17	180	6	4
Cephalothin	30	770	14	18	2	40
Nitrocefin	38	710	9	17	4	40
Imipenem	23	70	6	3	4	20

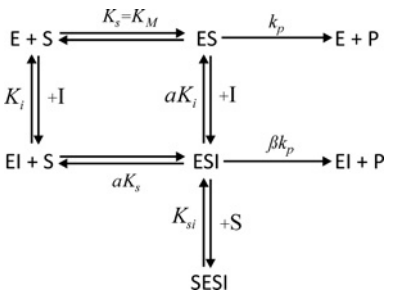

Scheme 1 Kinetic model of VIM-4 inhibition by the nanobody Nb-VIM38

$$v_i = \frac{k_{cat}E_0\left[1+\beta\frac{I}{\alpha K_i}\right]S}{K_m\left(1+\frac{I}{K_i}\right)+S\left(1+\frac{I}{\alpha K_i}+\frac{SI}{\alpha K_i K_{si}}\right)} \quad (1)$$

The k_{cat} constant is the turnover rate constant. K_m is the Henri–Michaelis–Menten constant, which is considered the dissociation constant for the substrate in this study. K_i and K_{si} are the dissociation constants for the inhibitor and a second substrate molecule respectively. The α parameter determines the degree at which the binding of the inhibitor modifies the affinity of the enzyme for the substrate. The β parameter defines the degree of activity of the ESI ternary complex compared with the activity of the ES complex. This complex model was compared with simpler models, in which substrate inhibition (K_{si}), competitive pathway (α) and partial behaviour (β) were successively ignored, through an Extra Sum of Squares F-test, which was performed using GraphPad Prism 5.04 software.

RESULTS

Preparation of VIM-4

A new protocol for the production of VIM-4 in a bioreactor, which allows the recovery of 20 mg of pure and stable protein per litre of culture, was developed. The development of this protocol revealed that the addition of metal ions at 10-fold the recommended concentration (a final concentration of 20 μM) to the auto-induction culture medium ZYM-5052 was critical to obtain a high production yield and a homogeneous VIM-4 preparation [24]. In addition, the catalytic efficiency of the VIM-4 produced using this protocol was 10-fold higher than that of the VIM-4 produced in the absence of additional Zn^{2+} (Table 1).

Phage display

Two libraries, a llama library of 2×10^8 cfu (colony-forming units) and a dromedary library of 2×10^7 cfu with nanobody gene insert rates of at least 85 and 96 % respectively, were obtained. The llama library was first panned on immobilized VIM-4 MβL adsorbed on MaxiSorp plates. The elutions were achieved by successive treatments with basic solution (1.4 % triethylamine). An enrichment of the VIM-4-specific phages was observed after two rounds of selection. Out of 144 randomly isolated colonies, more than 90 % were found to be positive by ELISA and 13 different sequences were identified. However, on the basis of CDR3 sequence similarities, only six of these nanobodies were significantly different from each other, and none of the 13 purified nanobodies displayed inhibitory activity towards VIM-4 (Supplementary Figure S1 at http://www.biochemj.org/bj/450/bj4500477add.htm).

We therefore decided to screen the llama and dromedary libraries in solution using biotinylated VIM-4 (sulfo-NHS-SS-biotin) in combination with streptavidin magnetic beads [27]. The elution of the phage–VIM-4 complexes was carried out in the presence of 50 mM DTT. Interestingly, only one round of selection was required to identify 23 and 20 new llama and dromedary nanobodies respectively. These new sequences were aligned and grouped according to their CDR3 sequence similarity. From sequence similarity analysis, six llama nanobodies and 14 dromedary nanobodies were expected to bind new epitopes on VIM-4. Of all of the purified binders, only one, the dromedary nanobody NbVIM_38, inhibited VIM-4 in the micromolar range. This antibody fragment displays the usual hallmarks of dromedary nanobodies, i.e. amino acids Phe^{42}, Gln^{49}, Arg^{50} and Gly^{52} in FR2 (framework 2), a long CDR3 composed of 20 amino acids [IMGT (International ImMunoGeneTics) numbering] and an additional disulfide bond that connects CDR1 to CDR3 [29]. The NbVIM_38 nanobody also inhibits VIM-2; thus, although no inhibition was observed with other MβLs (BcII, BlaB, L1 and CphA), it probably inhibits all of the members of the VIM subfamily. Using the original pHEN14 expression vector, no more than 1 mg of soluble nanobody per litre of TB medium was produced, and all attempts to attain increased concentrations of the nanobody failed. The nanobody sequence was therefore fused to the sequence of the rat cytochrome b_5 protein, which is referred to as the 'cherry protein'. This N-terminal fusion strategy allowed the purification of 90 mg of cherry–NbVIM_38 per litre of culture using an IMAC column.

Kinetic characterization

No significant difference was observed in the residual activity curves obtained with up to 10 μM of inhibitor using either NbVIM_38 alone or the fusion protein cherry–NbVIM_38. Therefore cherry–NbVIM_38 was used for a detailed analysis of VIM-4 inhibition by NbVIM_38 (Figure 2A, inset). VIM-4 hydrolyses various β-lactam families, such as carbapenems, penams and cephems. The activity of VIM-4 against imipenem, benzylpenicillin and cephalothin, one antibiotic from each family respectively, was inhibited in the presence of micromolar range

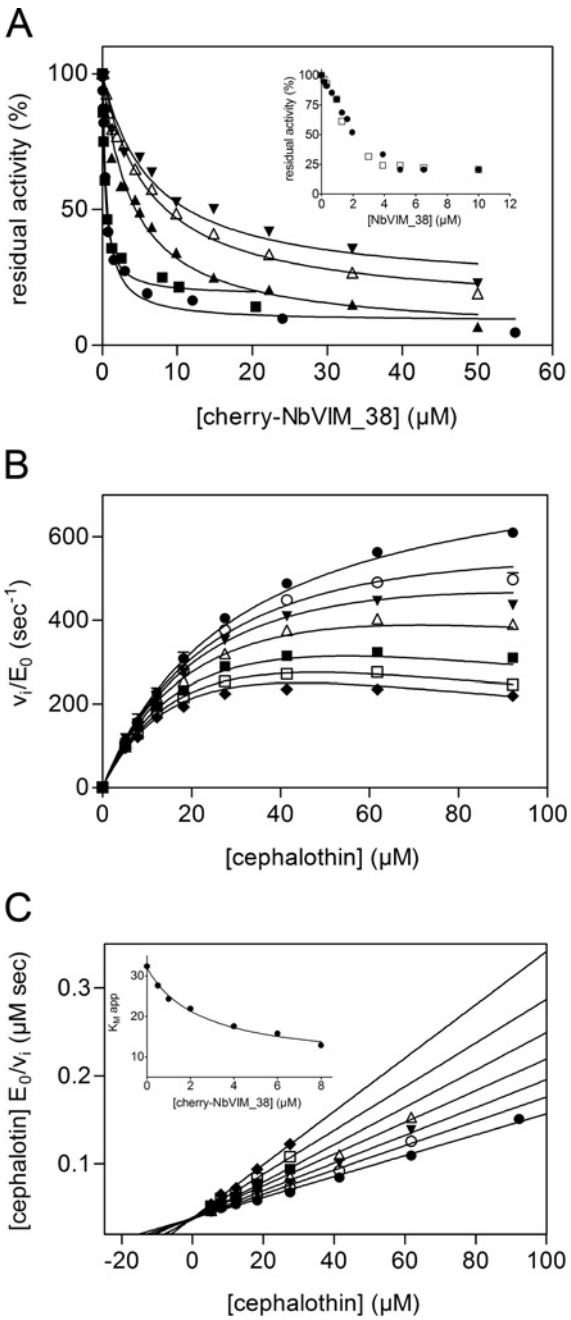

Figure 2 Steady-state study of VIM-4 inhibition by cherry–NbVIM_38

(**A**) Residual activity plot with 25 μM imipenem (●), 175 μM benzylpenicillin (■) and 15 μM (▼), 50 μM (△) and 80 μM (▲) cephalothin. Inset: residual activity plot with 18 μM nitrocefin showing the inhibition of VIM-4 by free NbVIM_38 (□) and the fused cherry–NbVIM_38 protein (●). (**B**) Influence of substrate concentration on the initial rate of cephalothin hydrolysis. Cherry–NbVIM_38 concentration: 0 (●), 0.5 (○), 1 (▼), 2 (△), 4 (■), 6 (□) and 8 (◆) μM. The continuous lines were drawn by performing a global fitting of eqn (1) to all of the datasets using the inhibitor concentrations as local constants. (**C**) Hanes–Woolf linearization of the inhibition curves. The data points corresponding to the substrate concentrations that were much larger than the apparent K_m were removed to highlight the convergence of the lines beyond the *y*-axis, which is typical of a predominantly uncompetitive mixed inhibition type. Cherry–NbVIM_38 concentration: 0 (●), 0.5 (○), 1 (▼), 2 (△), 4 (■), 6 (□) and 8 (◆) μM. Inset: apparent K_m ($-x_0$ of Hanes–Woolf lines) as a function of the concentration of cherry–NbVIM_38. The fitting was performed using the equation: $K_m(app) = K_m(1 + I/K_i)/(1 + I/\alpha K_i)$.

concentrations of cherry–NbVIM_38 (Figure 2A). This inhibition was more efficient at high substrate concentrations. In fact, the residual β-lactamase activity was lower at a cephalothin concentration of 80 μM (5-fold the K_m) than at concentrations of 50 or 15 μM. The Michaelis–Menten curves showed a decrease in both the apparent K_m and k_{cat} values with increasing inhibitor concentrations (Figure 2B). Because replots of the inhibition data showed hyperbolic curves, which is consistent with the residual activity plots, the ternary complex ESI was determined to retain some activity. Moreover, at higher concentrations of cherry–NbVIM_38, the Michaelis–Menten curves significantly deviated from rectangular hyperbola, which indicates that the binding of cherry–NbVIM_38 makes the cephalothin substrate behave as an inhibitor at high concentrations to yield a catalytically inactive SESI complex. Interestingly, in the absence of inhibitor, this phenomenon was not observed at cephalothin concentrations up to 400 μM (Supplementary Figure S2 at http://www.biochemj.org/bj/450/bj4500477add.htm). The Hanes–Woolf linearization also visualized this phenomenon and suggests that the inhibition observed with cherry–NbVIM_38 follows the kinetics of a mixed inhibition model with a significant uncompetitive component, i.e. the binding of the inhibitor promotes substrate binding and reciprocally (Figure 2C). Therefore the model illustrated in Scheme 1, which was used to derive eqn (1), was chosen. A global analysis of the Michaelis–Menten curves using this equation was then performed. The derived parameters are shown in Table 2.

Table 2 Steady-state inhibition parameters

The parameters were obtained through a global analysis of the Michaelis–Menten curves using eqn (1). $R^2 = 0.9954$. Values are means ± S.D.

k_{cat} (s^{-1})	K_m (μM)	α	β	K_i (μM)	K_{si} (μM)
820 ± 17	31 ± 2	0.6 ± 0.2	0.4 ± 0.1	9 ± 2	45 ± 14

The parameters α and β confirmed a predominantly uncompetitive ($\alpha < 1$) and partial ($0 < \beta < 1$) mixed inhibition model with dissociation constants for the inhibitor, K_i, and the second cephalothin molecule, K_{si}, of 9 and 45 μM respectively.

This complex model was compared with simpler models, in which the substrate inhibition (K_{si}) and partial behaviour (β) were ignored, through Extra Sum of Squares F-tests. In each comparison, the preferred model was the complete model shown in Scheme 1 ($P < 0.0001$). Compared with the simpler models, the complete model attained the highest R^2 (0.9954). In addition, the residuals of the complete model were the residuals that were most randomly scattered around zero.

Alanine scanning of the paratope

A series of alanine substitutions were introduced into the CDR2 and CDR3 loops of NbVIM_38 to identify the amino acids that are essential for the inhibition of VIM-4 (Figure 3A). The amino acids Pro^{111}, $Cys^{111.1}$, $Pro^{112.4}$ and $Gly^{112.3}$, were not mutated because these residues are likely to be critical for the loop conformation of CDR3. In fact, $Cys^{111.1}$ of CDR3 and Cys^{38} of CDR1 are probably involved in a disulfide bond; in addition, the residues $Pro^{122.4}$ and $Gly^{112.3}$, which have restrained and extended dihedral angle combinations respectively, are also presumably important in the conformation of the CDR3 loop.

Seventeen mutants were purified, and their inhibitory abilities were assessed in microplates at a final concentration of 5 μM using nitrocefin as the substrate. The residual activities were converted into inhibition percentages to obtain the histogram shown in Figure 3(B). In the CDR2 loop, only Arg^{58} and Gly^{62}

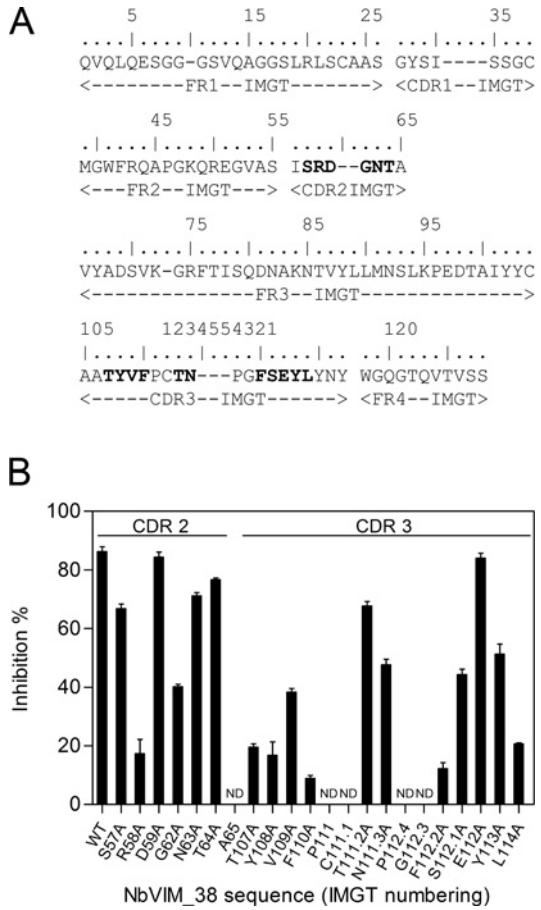

Figure 3 Analysis of the paratope

(**A**) Amino acid sequence of the NbVIM_38 nanobody. The residues subjected to alanine scanning are in bold (IMGT numbering). (**B**) Alanine scan of the NbVIM_38 paratope. The residual activities were converted into inhibition percentages. ND, not determined.

were found to be essential for efficient inhibition of the MβL. Most of the mutations that affected the inhibition of VIM-4 were found in the CDR3 loop. The four consecutive residues located before Cys$^{111.1}$ in the N-terminal region of CDR3 are hydrophobic amino acids (Thr^{107}, Tyr^{108}, Val^{109} and Phe^{110}), and their substitution led to a decrease (60–90 %) in the inhibitory strength of the nanobody. It can therefore be hypothesized that these residues are located within the binding interface of the complex that is formed between cherry–NbVIM_38 and VIM-4. Two additional hydrophobic amino acids (Phe$^{112.2}$ and Leu^{114}) found in the C-terminal region of the CDR3 loop were also found to be critical for binding. Residues Ser$^{112.1}$ and Tyr^{113} also seem to participate in the interaction because their substitution resulted in an observed reduction in the inhibitory potency.

Epitope mapping

In order to identify the epitope that is recognized by the NbVIM_38 nanobody, a scanning peptide array of dodecapeptides covering the entire sequence of VIM-4 was constructed and analysed by immunodetection. Six consecutive spots, whose signals were most saturated, and which corresponded to the Ile^{99}–Gly^{133} (class B β-lactamase numbering) region of the VIM-4 MβL, were clearly identified (B line, Figure 4A). However, non-specific signals, including peptide D11 as well as peptide D25, which was a scrambled peptide used as negative control, were also visible. Therefore, in order to confirm and refine the epitope mapping result, the binding of cherry–NbVIM_38 on a set of overlapping biotinylated peptides corresponding to the sequence identified on the peptide array was assayed by ELISA (Figure 4B). This latter experiment confirmed that the identified epitope starts at the end of the α1 helix (A^{97}EIEKQ^{102}) and successively encompasses the exposed L6 loop (I^{103}GLPVTR^{111}), the small β5 strand (A^{112}VS^{114}), the active-site L7 loop (T^{115}HFHDDR^{121}) and the distorted α2 helix (V^{122}GGVDVLRAAG^{133}) (Figure 4C). The control peptide 1, which was the same as peptide D11 on the peptide array, as well as the control peptide 2, which was a scrambled peptide, was clearly negative. Moreover, on the basis of a comparison between signal intensities for peptides, two exposed stretches of amino acids, i.e. LPVTRA and VLRAAG, were highlighted and were expected to be the main binding determinants. Interestingly, these two hexapeptides were also the two shortest peptides still being recognized by cherry–NbVIM_38 in a truncation analysis performed by peptide array (Supplementary Figure S3 at http://www.biochemj.org/bj/450/bj4500477add.htm).

As a last confirmation, a functional chimaeric protein named VIMΔepitope, which corresponds to the VIM-4 MβL protein except that the Ile^{99}–Gly^{133} sequence of VIM-4 has been replaced by the corresponding sequence from the MβL BlaB, was produced (Supplementary Figure S2). In ELISA experiments, this chimaeric MβL did not bind to cherry–NbVIM_38 (Figure 5A). In addition, an enzymatic assay did not reveal any inhibition, which confirms that the Ile^{99}–Gly^{133} sequence contains the epitope. Therefore the side chains that are responsible for binding are from exposed amino acids that differ between the two substituted sequences of BlaB and VIM-4. These are LPVTRA (L6) and DVLRAAG (α2), which was in line with the results obtained by the immunodetection experiments (Figure 5B). In the crystallographic structure of VIM-4, these two peptides, which would constitute the core of this conformational epitope, coincide with exposed sequences that are in close proximity to each other (L6 loop and the C-terminus of the α2 helix), but distant from the active site (Figure 5C). In contrast, the sequence corresponding to the active-site L7 loop followed by the N-terminal part of the α2 helix (THFHDDRVGGVD; peptide 5 analysed in Figure 5B), which is well conserved between MβLs, is not directly involved in the binding. This could also be deduced from the peptide truncation analysis (Supplementary Figure S3).

DISCUSSION

The aim of the present study was to obtain nanobodies that inhibit MβLs and could eventually be further minimized to obtain lead peptides. Therefore a llama and a dromedary were immunized with the MβL VIM-4, a member of the clinically relevant VIM family.

The first screening of the llama library most probably failed because of the low diversity of the selected binders (13 nanobodies), all of which lacked inhibitory properties. It was therefore decided to also screen a dromedary library mainly for two reasons. First, most of nanobodies that have been described as enzyme inhibitors originate from dromedaries [14,17–21]. Secondly, it has been shown that dromedary nanobodies, which have been classified into a different subfamily by Harmsen et al. [30], often exhibit different properties, such as an additional disulfide bridge and a longer CDR3. These hallmarks could result in a preference for different epitopes, such as grooves and clefts on

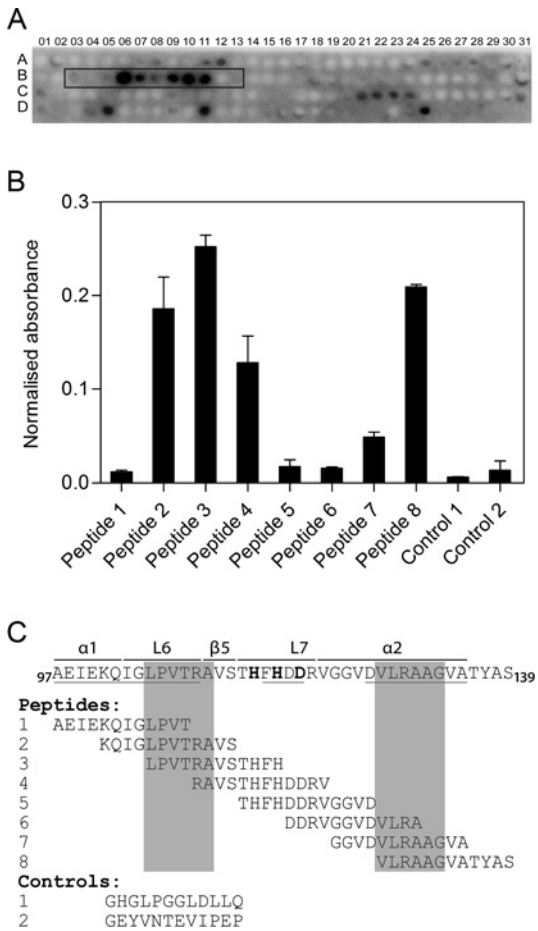

Figure 4 Epitope mapping of the NbVIM_38 nanobody

(**A**) Peptide array that covers the entire amino acid sequence of VIM-4. Spots B3 to B13 (boxed) correspond to peptides that define the epitope of the NbVIM_38 nanobody. The experiment was performed in duplicate, and both arrays gave the same result. (**B**) ELISA analysis of the binding to cherry–NbVIM_38 of the biotinylated peptides that were identified on the peptide array. The histogram illustrates the results of three independent experiments. Values are means ± S.D. (**C**) Amino acid sequence of the epitope aligned with the overlapping peptides that were analysed in the ELISA experiment. The secondary structures are labelled, the Zn^{2+}-co-ordinating amino acids are shown in bold, and the solvent-exposed residues are underlined. The exposed amino acids stretches that are believed to be the main binding determinants are highlighted using dark grey shading. Control peptide 1 is the same as peptide D11 on the peptide array and control peptide 2 is a random peptide used as a negative control.

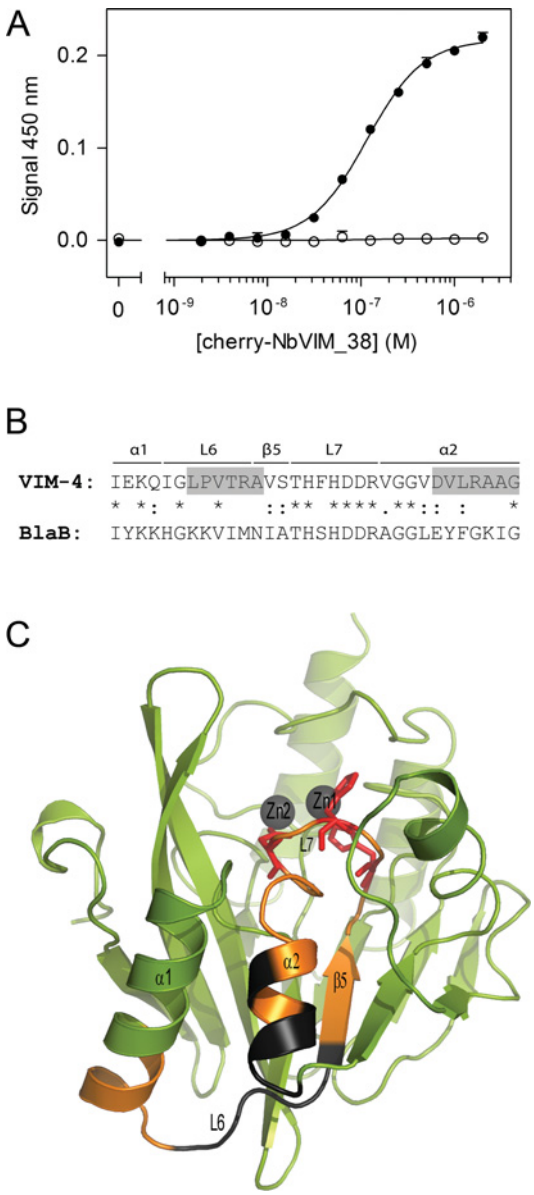

Figure 5 Epitope of the NbVIM_38 nanobody

(**A**) ELISA experiment with coated WT VIM-4 (●) and coated VIMΔepitope (○). (**B**) Alignment of the VIM-4 epitope sequence and the corresponding BlaB sequence. The amino acid stretches that are thought to be the main binding determinants are shaded in grey. (**C**) Crystallographic structure of VIM-4 (PDB code 2WHG). The epitope region Ile^{99}–Gly^{133}, is shown in orange. The amino acid stretches LPVTRA and VLRAAG are displayed in black. The Zn^{2+} ions are represented by grey spheres. The Zn^{2+}-co-ordinating amino acids of the L7 loop are shown as red sticks.

the antigen surface [16]. Moreover, it is likely that the utilization of non-specific elutions of phages resulted in the convergence of the library towards high-affinity binders that were devoid of inhibitory ability. In addition, the fold of VIM-4 could be altered upon the adsorption on to the microlitre plate, thereby preventing the selection of conformational inhibitory binders. For these reasons, the screening procedure was modified to perform the panning procedure in solution using biotinylated VIM-4 [27]. The phage–antigen complexes were eluted with a DTT solution, which was accomplished as a result of a disulfide bridge in the biotin linker. This specific elution protocol resulted in an enrichment of the library after only one selection round, thus allowing the selection of a more diverse set of 43 new sequences. Out of these, the dromedary NbVIM_38 nanobody was found to be the only inhibitor of VIM-4.

The NbVIM_38 nanobody was not easily produced and purified. Therefore the so-called 'cherry protein' was fused to its N-terminus. A concentration of 10 μM of either the fusion protein or free nanobody inhibited 80 % of VIM-4 activity using nitrocefin as a reporter substrate (Figure 2A, inset). It is thus likely that the inhibition model shown in Scheme 1 is valid for both proteins. However, because inhibition data at high NbVIM_38 concentrations could not be obtained, it is still possible that the nanobody behaves differently when it is used alone.

The Michaelis–Menten saturation curves at different inhibitor concentrations were complicated by the superimposition of two types of inhibition, i.e. a predominantly uncompetitive partial mixed-inhibition, which gave rise to a hyperbolic replot of the

inhibition data, and a substrate inhibition that only occurred when cherry–NbVIM_38 was bound (Figure 2B). This superimposition resulted in a decrease in the apparent K_m values for cephalothin (Figure 2C, inset, and Table 2). The minimal model that describes these data is illustrated by Scheme 1. As the nanobody binds to the enzyme, its affinity for cephalothin rises (uncompetitive tendency, $\alpha < 1$), and the binding to a second cephalothin molecule results in substrate inhibition.

Substrate inhibition occurs when a second substrate molecule binds to the enzyme and blocks its activity. This type of inhibition has been observed previously for other MβLs, such as CcrA [31], Mb11b [32], IMP-1 S121G and F218Y mutants [33]. In the present study, a second substrate molecule was found to bind to the ESI complex to yield the inactive SESI complex, as shown in Scheme 1. This inhibition mechanism suggests the presence of an inhibitor binding site outside of the active-site pocket that alters its geometry and/or dynamics such that it allows the binding of a second inhibitory substrate molecule.

The paratope of NbVIM_38, with the exception of the CDR1 loop, was investigated using alanine scanning to identify the residues that are important for binding (Figure 3B). The CDR3 of NbVIM_38 is mainly composed of hydrophobic amino acids, which suggests that the binding of the nanobody is mediated by hydrophobic interactions. Consistent with this observation, each substitution of one of the four consecutive hydrophobic residues $T^{107}YVF^{110}$ greatly reduced the inhibition of VIM-4. This amino acid stretch is probably located within the binding interface of the complex. Moreover, as observed in many crystallographic structures of nanobodies, the C-terminal region of CDR3 after the disulfide bridge (Cys^{38}–Cys^{111}) probably folds over the VL side of the domain to shield the hydrophobic amino acids of FR2 from the solvent [34]. Therefore we hypothesize that $Phe^{112.2}$ and Leu^{114} interact with FR2 and that this interaction confers an adequate conformation to the CDR3 loop that enables the interaction with VIM-4, which occurs mainly through amino acids Thr^{107}–Phe^{110}. This conformation would also allow $Ser^{112.1}$ and Tyr^{113} to participate in the stabilization of the complex in synergy with other amino acids, such as Arg^{58} in the CDR2.

All attempts to crystallize the VIM-4–NbVIM_38 complex failed. Therefore epitope mapping was performed using a scanning peptide array and an ELISA (Figure 4). These two experiments allowed the identification of the Ile^{99}–Gly^{133} sequence of VIM-4 that contains the main binding determinants. Substitution of this sequence with the corresponding one of another MβL (BlaB) yielded the functional chimaera VIMΔepitope, which was not recognized by the nanobody (Figure 5A and Supplementary Figure S2). This latter experiment and the comparison between ELISA signal intensities for peptides also highlighted the importance of two stretches of amino acids, i.e. LPVTRA and VLRAAG. These two exposed sequences are close to each other in the crystallographic structure of VIM-4 and correspond respectively to the L6 loop and to the end of the α2 helix (Figure 5C). Therefore these two stretches, which define a hydrophobic pocket together with the amphiphilic α1 helix, are probably located within the binding interface of the VIM-4–NbVIM_38 complex, and would correspond to the core of this conformational epitope. In contrast, the active-site L7 loop and the N-terminal part of the α2 helix are probably not directly involved in the binding of the nanobody to VIM-4. This view is supported by additional observations. First, although the active-site loop L7 are highly similar among all B1 MβLs, the inhibition by cherry–NbVIM_38 was restricted to VIM MβLs. Secondly, the active-site loop L7 is electrophilic, whereas the paratope of NbVIM_38 suggests a binding event that is mainly driven by hydrophobic interactions (Figure 3). Thirdly, a nanobody paratope cannot cover a surface that would include the L7 active-site loop, the L6 loop (LPVTRA) and the end of the α2 helix (VLRAAG). Finally, the mode of inhibition was found to be predominantly uncompetitive, which does not favour an inhibitor-binding site that includes an active-site loop involved in zinc co-ordination and substrate binding.

Because the NbVIM_38 nanobody binds to a site that is distant from the active site and alters both the VIM-4 substrate binding and catalytic properties, this nanobody behaves as an allosteric effector for which the kinetic parameters α and β (Table 2) quantify its allosteric coupling [35]. Allosteric behaviour implies that conformational and/or dynamic changes of the allosteric residues ultimately affect the active site [36]. The dynamic nature of MβLs can already be inferred from their active sites made of loops which allow the catalysis of a wide range of differently substituted β-lactams through the formation of different intermediates [37–41]. Similarly, mutations of residues that are distant from the active site and that enhance the catalytic efficiency cannot be understood unless flexibility and motion are integral components of their mechanism [33,42]. In directed evolution studies that were performed on the BcII MβL, Tomatis et al. [43,44] obtained four high-frequency mutations that alter the cephalosporinase activity. None of these mutations were directly involved in metal co-ordination or substrate binding. Among them, the mutation V112A, which lies at the end of loop L6, was the only mutation that was present in 100 % of the selected clones. Its systematic presence was interpreted as indirect evidence of the existence of molecular motion in the active site that is coupled to remote positions in the structure.

Other biophysical results have demonstrated the flexible and dynamic nature of MβLs, and some of these studies also highlighted residues that are located in the epitope sequence that is recognized by NbVIM_38. In addition to the well-characterized flexibility of the so-called flapping loop (L3), which is thought to be the main determinant of the active-site plasticity [45], NMR, MD (molecular dynamics) simulations and X-ray crystallography [10], have shed more light on the flexibility of the L7 and L10 loops, which are both involved in metal co-ordination. MD simulations identified a localized flip in the L7 loop of the CcrA MβL that was consistent with previously observed NMR chemical shifts of the same enzyme [46,47]. This localized change of conformation would result from the increased Zn–Zn distance upon the binding of a ligand to the active site. This increased Zn–Zn distance was also observed by EXAFS (extended X-ray absorption fine structure) spectroscopy [48,49], and in crystal structures of MβLs that are complexed with hydrolysed substrates [39,50–52]. Two conserved glycine residues, which distort the N-terminal part of the α2 helix in all B1 and B2 MβLs, could confer the required flexibility to the L7 loop and enable it to undergo the necessary change in the active-site geometry during catalysis. A similar role for the glycine residues in the vicinity of other Zn^{2+}-co-ordinating amino acids has already been assigned for MβLs [10,44]. Therefore it is tempting to hypothesize that the binding of the NbVIM_38 nanobody inhibits VIM-4 by interfering with the dynamic of the L7 loop. Other experiments, such as relaxation NMR and X-ray crystallography of the complex, are required to test this hypothesis further.

In conclusion, we selected 56 different nanobodies that recognize the clinically relevant VIM-4 MβL. Out of these, the NbVIM_38 nanobody behaves as an allosteric inhibitor of VIM-4 because it displays partial mixed inhibition and interacts with an epitope that is distant from the active site. This inhibition indirectly underlines the dynamic nature of MβLs, which allows their allosteric regulation by an antibody fragment.

AUTHOR CONTRIBUTION

Jean S. Sohier conducted all of the experiments and wrote the paper. Clémentine Laurent participated in the alanine scanning of the paratope and the kinetic characterization of the inhibition. Andy Chevigné designed the peptide array, helped with the analysis of the epitope mapping results and commented the paper. Els Pardon and Vasundara Srinivasan assisted with the phage display experiment. Ulrich Wernery performed the immunization of the dromedary. Patricia Lassaux gave 2 mg of VIM-4 used only for the first round of llama immunization. Jan Steyaert and Moreno Galleni supervised the project and wrote the paper.

ACKNOWLEDGEMENTS

We thank Nele Buys and Katleen Willibal for their technical help concerning phage display experiments, and Professor Jean-Marie Frère and Dr Frédéric Sapunaric for helpful discussions on enzyme kinetics.

FUNDING

This work was supported by the Centre de Recherche Public-Santé, Luxembourg [grant number 20100708, GPCR47 project)], and Interuniversity Attraction Poles [grant number P6/19 (to E.P.)]. J.S.S. is an FRIA (Fonds pour la formation à la Recherche dans l'Industrie et dans l'Agriculture) Fellow of F.R.S. (Fonds pour la Recherche Scientifique)-FNRS (Belgium).

REFERENCES

1 Ambler, R. P. (1980) The structure of β-lactamases. Philos. Trans. R. Soc. London Ser. B **289**, 321–331
2 Galleni, M., Lamotte-Brasseur, J., Rossolini, G. M., Spencer, J., Dideberg, O. and Frere, J. M. (2001) Standard numbering scheme for class B β-lactamases. Antimicrob. Agents Chemother. **45**, 660–663
3 Carfi, A., Pares, S., Duee, E., Galleni, M., Duez, C., Frere, J. M. and Dideberg, O. (1995) The 3-D structure of a zinc metallo-β-lactamase from *Bacillus cereus* reveals a new type of protein fold. EMBO J. **14**, 4914–4921
4 Bebrone, C. (2007) Metallo-β-lactamases (classification, activity, genetic organization, structure, zinc coordination) and their superfamily. Biochem. Pharmacol. **74**, 1686–1701
5 Garau, G., Garcia-Saez, I., Bebrone, C., Anne, C., Mercuri, P., Galleni, M., Frere, J. M. and Dideberg, O. (2004) Update of the standard numbering scheme for class B β-lactamases. Antimicrob. Agents Chemother. **48**, 2347–2349
6 Cornaglia, G., Giamarellou, H. and Rossolini, G. M. (2011) Metallo-β-lactamases: a last frontier for β-lactams? Lancet Infect. Dis. **11**, 381–393
7 Walsh, T. R., Toleman, M. A., Poirel, L. and Nordmann, P. (2005) Metallo-β-lactamases: the quiet before the storm? Clin. Microbiol. Rev. **18**, 306–325
8 Bush, K. and Fisher, J. F. (2011) Epidemiological expansion, structural studies, and clinical challenges of new β-lactamases from Gram-negative bacteria. Annu. Rev. Microbiol. **65**, 455–478
9 Llarrull, L. I., Tioni, M. F. and Vila, A. J. (2008) Metal content and localization during turnover in *B. cereus* metallo-β-lactamase. J. Am. Chem. Soc. **130**, 15842–15851
10 Gonzalez, J. M., Buschiazzo, A. and Vila, A. J. (2010) Evidence of adaptability in metal coordination geometry and active-site loop conformation among B1 metallo-β-lactamases. Biochemistry **49**, 7930–7938
11 Bebrone, C., Lassaux, P., Vercheval, L., Sohier, J. S., Jehaes, A., Sauvage, E. and Galleni, M. (2010) Current challenges in antimicrobial chemotherapy: focus on β-lactamase inhibition. Drugs **70**, 651–679
12 Drawz, S. M. and Bonomo, R. A. (2010) Three decades of β-lactamase inhibitors. Clin. Microbiol. Rev. **23**, 160–201
13 Perez-Llarena, F. J. and Bou, G. (2009) β-Lactamase inhibitors: the story so far. Curr. Med. Chem. **16**, 3740–3765
14 Conrath, K. E., Lauwereys, M., Galleni, M., Matagne, A., Frere, J. M., Kinne, J., Wyns, L. and Muyldermans, S. (2001) β-Lactamase inhibitors derived from single-domain antibody fragments elicited in the camelidae. Antimicrob. Agents Chemother. **45**, 2807–2812
15 Muyldermans, S., Cambillau, C. and Wyns, L. (2001) Recognition of antigens by single-domain antibody fragments: the superfluous luxury of paired domains. Trends Biochem. Sci. **26**, 230–235
16 De Genst, E., Silence, K., Decanniere, K., Conrath, K., Loris, R., Kinne, J., Muyldermans, S. and Wyns, L. (2006) Molecular basis for the preferential cleft recognition by dromedary heavy-chain antibodies. Proc. Natl. Acad. Sci. U.S.A. **103**, 4586–4591
17 Conrath, K., Pereira, A. S., Martins, C. E., Timoteo, C. G., Tavares, P., Spinelli, S., Kinne, J., Flaudrops, C., Cambillau, C., Muyldermans, S. et al. (2009) Camelid nanobodies raised against an integral membrane enzyme, nitric oxide reductase. Protein Sci. **18**, 619–628
18 Desmyter, A., Spinelli, S., Payan, F., Lauwereys, M., Wyns, L., Muyldermans, S. and Cambillau, C. (2002) Three camelid VHH domains in complex with porcine pancreatic α-amylase. Inhibition and versatility of binding topology. J. Biol. Chem. **277**, 23645–23650
19 Lauwereys, M., Arbabi Ghahroudi, M., Desmyter, A., Kinne, J., Holzer, W., De Genst, E., Wyns, L. and Muyldermans, S. (1998) Potent enzyme inhibitors derived from dromedary heavy-chain antibodies. EMBO J. **17**, 3512–3520
20 Transue, T. R., De Genst, E., Ghahroudi, M. A., Wyns, L. and Muyldermans, S. (1998) Camel single-domain antibody inhibits enzyme by mimicking carbohydrate substrate. Proteins **32**, 515–522
21 Barlow, J. N., Conrath, K. and Steyaert, J. (2009) Substrate-dependent modulation of enzyme activity by allosteric effector antibodies. Biochim. Biophys. Acta **1794**, 1259–1268
22 Oyen, D., Srinivasan, V., Steyaert, J. and Barlow, J. N. (2011) Constraining enzyme conformational change by an antibody leads to hyperbolic inhibition. J. Mol. Biol. **407**, 138–148
23 Pournaras, S., Maniati, M., Petinaki, E., Tzouvelekis, L. S., Tsakris, A., Legakis, N. J. and Maniatis, A. N. (2003) Hospital outbreak of multiple clones of *Pseudomonas aeruginosa* carrying the unrelated metallo-β-lactamase gene variants blaVIM-2 and blaVIM-4. J. Antimicrob. Chemother. **51**, 1409–1414
24 Studier, F. W. (2005) Protein production by auto-induction in high density shaking cultures. Protein Expression Purif. **41**, 207–234
25 Lassaux, P., Traore, D. A., Loisel, E., Favier, A., Docquier, J. D., Sohier, J. S., Laurent, C., Bebrone, C., Frere, J. M., Ferrer, J. L. and Galleni, M. (2011) Biochemical and structural characterization of the subclass B1 metallo-β-lactamase VIM-4. Antimicrob. Agents Chemother. **55**, 1248–1255
26 Arbabi Ghahroudi, M., Desmyter, A., Wyns, L., Hamers, R. and Muyldermans, S. (1997) Selection and identification of single domain antibody fragments from camel heavy-chain antibodies. FEBS Lett. **414**, 521–526
27 Chames, P., Hoogenboom, H. R. and Henderikx, P. (2002) Selection of antibodies against biotinylated antigens. Methods Mol. Biol. **178**, 147–157
28 Thys, B., Schotte, L., Muyldermans, S., Wernery, U., Hassanzadeh-Ghassabeh, G. and Rombaut, B. (2010) *In vitro* antiviral activity of single domain antibody fragments against poliovirus. Antiviral Res. **87**, 257–264
29 Muyldermans, S., Baral, T. N., Retamozzo, V. C., De Baetselier, P., De Genst, E., Kinne, J., Leonhardt, H., Magez, S., Nguyen, V. K., Revets, H. et al. (2009) Camelid immunoglobulins and nanobody technology. Vet. Immunol. Immunopathol. **128**, 178–183
30 Harmsen, M. M., Ruuls, R. C., Nijman, I. J., Niewold, T. A., Frenken, L. G. and de Geus, B. (2000) Llama heavy-chain V regions consist of at least four distinct subfamilies revealing novel sequence features. Mol. Immunol. **37**, 579–590
31 Yanchak, M. P., Taylor, R. A. and Crowder, M. W. (2000) Mutational analysis of metallo-β-lactamase CcrA from *Bacteroides fragilis*. Biochemistry **39**, 11330–11339
32 Simm, A. M., Higgins, C. S., Pullan, S. T., Avison, M. B., Niumsup, P., Erdozain, O., Bennett, P. M. and Walsh, T. R. (2001) A novel metallo-β-lactamase, Mbl1b, produced by the environmental bacterium *Caulobacter crescentus*. FEBS Lett. **509**, 350–354
33 Oelschlaeger, P., Mayo, S. L. and Pleiss, J. (2005) Impact of remote mutations on metallo-β-lactamase substrate specificity: implications for the evolution of antibiotic resistance. Protein Sci. **14**, 765–774
34 Muyldermans, S. and Lauwereys, M. (1999) Unique single-domain antigen binding fragments derived from naturally occurring camel heavy-chain antibodies. J. Mol. Recognit. **12**, 131–140
35 Fenton, A. W. (2008) Allostery: an illustrated definition for the 'second secret of life'. Trends Biochem. Sci. **33**, 420–425
36 Kern, D. and Zuiderweg, E. R. (2003) The role of dynamics in allosteric regulation. Curr. Opin. Struct. Biol. **13**, 748–757
37 Garau, G., Bebrone, C., Anne, C., Galleni, M., Frere, J. M. and Dideberg, O. (2005) A metallo-β-lactamase enzyme in action: crystal structures of the monozinc carbapenemase CphA and its complex with biapenem. J. Mol. Biol. **345**, 785–795
38 McManus-Munoz, S. and Crowder, M. W. (1999) Kinetic mechanism of metallo-β-lactamase L1 from *Stenotrophomonas maltophilia*. Biochemistry **38**, 1547–1553
39 Spencer, J., Read, J., Sessions, R. B., Howell, S., Blackburn, G. M. and Gamblin, S. J. (2005) Antibiotic recognition by binuclear metallo-β-lactamases revealed by X-ray crystallography. J. Am. Chem. Soc. **127**, 14439–14444
40 Tioni, M. F., Llarrull, L. I., Poeylaut-Palena, A. A., Marti, M. A., Saggu, M., Periyannan, G. R., Mata, E. G., Bennett, B., Murgida, D. H. and Vila, A. J. (2008) Trapping and characterization of a reaction intermediate in carbapenem hydrolysis by *B. cereus* metallo-β-lactamase. J. Am. Chem. Soc. **130**, 15852–15863

41 Wang, Z., Fast, W. and Benkovic, S. J. (1999) On the mechanism of the metallo-β-lactamase from *Bacteroides fragilis*. Biochemistry **38**, 10013–10023
42 Oelschlaeger, P. and Pleiss, J. (2007) Hydroxyl groups in the $\beta\beta$ sandwich of metallo-β-lactamases favor enzyme activity: Tyr218 and Ser262 pull down the lid. J. Mol. Biol. **366**, 316–329
43 Tomatis, P. E., Rasia, R. M., Segovia, L. and Vila, A. J. (2005) Mimicking natural evolution in metallo-β-lactamases through second-shell ligand mutations. Proc. Natl. Acad. Sci. U.S.A. **102**, 13761–13766
44 Tomatis, P. E., Fabiane, S. M., Simona, F., Carloni, P., Sutton, B. J. and Vila, A. J. (2008) Adaptive protein evolution grants organismal fitness by improving catalysis and flexibility. Proc. Natl. Acad. Sci. U.S.A. **105**, 20605–20610
45 Huntley, J. J., Fast, W., Benkovic, S. J., Wright, P. E. and Dyson, H. J. (2003) Role of a solvent-exposed tryptophan in the recognition and binding of antibiotic substrates for a metallo-β-lactamase. Protein Sci. **12**, 1368–1375
46 Salsbury, Jr, F. R., Crowder, M. W., Kingsmore, S. F. and Huntley, J. J. (2009) Molecular dynamic simulations of the metallo-β-lactamase from *Bacteroides fragilis* in the presence and absence of a tight-binding inhibitor. J. Mol. Model. **15**, 133–145
47 Scrofani, S. D., Chung, J., Huntley, J. J., Benkovic, S. J., Wright, P. E. and Dyson, H. J. (1999) NMR characterization of the metallo-β-lactamase from *Bacteroides fragilis* and its interaction with a tight-binding inhibitor: role of an active-site loop. Biochemistry **38**, 14507–14514
48 Costello, A., Periyannan, G., Yang, K. W., Crowder, M. W. and Tierney, D. L. (2006) Site-selective binding of Zn(II) to metallo-β-lactamase L1 from *Stenotrophomonas maltophilia*. J. Biol. Inorg. Chem. **11**, 351–358
49 Breece, R. M., Hu, Z., Bennett, B., Crowder, M. W. and Tierney, D. L. (2009) Motion of the zinc ions in catalysis by a dizinc metallo-β-lactamase. J. Am. Chem. Soc. **131**, 11642–11643
50 Ullah, J. H., Walsh, T. R., Taylor, I. A., Emery, D. C., Verma, C. S., Gamblin, S. J. and Spencer, J. (1998) The crystal structure of the L1 metallo-β-lactamase from *Stenotrophomonas maltophilia* at 1.7 Å resolution. J. Mol. Biol. **284**, 125–136
51 Zhang, H. and Hao, Q. (2011) Crystal structure of NDM-1 reveals a common β-lactam hydrolysis mechanism. FASEB J. **25**, 2574–2582
52 King, D. and Strynadka, N. (2011) Crystal structure of New Delhi metallo-β-lactamase reveals molecular basis for antibiotic resistance. Protein Sci. **20**, 1484–1491

Received 17 August 2012/11 December 2012; accepted 7 January 2013
Published as BJ Immediate Publication 7 January 2013, doi:10.1042/BJ20121305

Biochem. J. (2013) **450**, 477–486 (Printed in Great Britain) doi:10.1042/BJ20121305

online data

SUPPLEMENTARY ONLINE DATA
Allosteric inhibition of VIM metallo-β-lactamases by a camelid nanobody

Jean S. SOHIER*, Clémentine LAURENT*, Andy CHEVIGNÉ†, Els PARDON‡§, Vasundara SRINIVASAN‡§, Ulrich WERNERY‖, Patricia LASSAUX*, Jan STEYAERT‡§ and Moreno GALLENI*[1]

*Centre for Protein Engineering, Macromolecules Biologiques Unit, University of Liège, Allée du 6 Août, 13 (B6A), Sart-Tilman, 4000 Liege, Belgium, †Public Research Centre for Health (CRP-Santé), Laboratory of Retrovirology, Val Fleuri 84, L-1526 Luxembourg, Luxembourg, ‡Department of Structural Biology (VIB), Pleinlaan 2, 1050 Brussels, Belgium, §Structural Biology Brussels, Vrije Universiteit Brussel, Pleinlaan 2, 1050 Brussels, Belgium, and ‖Central Veterinary Research Laboratory, P.O. Box 597, Dubai, United Arab Emirates

EXPERIMENTAL

Chemicals and enzymes

The oligonucleotides and restriction enzymes were obtained from Eurogentec and Promega respectively. The amino acid derivatives and TIPS (tri-isopropylsilane) were purchased from Merck. DIC (*N*,*N*'-diisopropylcarbodiimide), HObt (1-hydroxybenzotriazole hydrate), acetic acid anhydride and DCM (dichloromethane) were obtained from Fluka. DMF (*N*,*N*-dimethylformamide), NMP (1-methyl-2-pyrrolidinone), piperidine and TFA (trifluoroacetic acid) were purchased from Sigma–Aldrich.

Phage selection in microlitre plates

For the selection of phages on solid-phase coated antigen, 100 μg/ml VIM-4 was immobilized in 96-well MaxiSorp plates through direct coating. The phages expressing the cloned nanobody repertoire were then incubated with the immobilized VIM-4 in 250 μl of PBS with 1 % non-fat dried skimmed milk for 10 min. The incubation was followed by 15 consecutive washes with PBST to remove any unbound phages. The bound phages were eluted by two successive treatments with 100 μl of 1.4 % TEA (triethylamine) and 100 μl of exponentially growing TG1 cells. A 10 μl aliquot of the eluted phages was used to evaluate the enrichment by comparing the number of eluted phages with or without antigen. The remaining phages were used to infect fresh exponentially growing cultures of *E. coli* TG1 cells, which were then rescued by superinfection with M13K07 helper phages, amplified and used for further rounds of panning. Two consecutive selection steps were needed to obtain a significant enrichment of anti-VIM-4 nanobodies.

Typically, after each selection process, 48 colonies were randomly chosen and grown in TB medium in the presence of 1 mM IPTG to induce the expression of the corresponding soluble nanobody in the periplasmic space. The crude periplasmic extracts were tested for their recognition of VIM-4 by ELISA. The nanobody genes from the positive clones were amplified by PCR. Restriction-length polymorphism analysis of the different nanobody genes was performed by digesting the amplimers with HinfI. The different predicted fingerprints were confirmed by DNA sequencing, and the amino acid sequences were aligned with ClustalW. On the basis of this alignment, 24 representative nanobodies were cloned into a Chl^R pHEN14 vector for expression with a His-tag in *E. coli*.

Table S1 Oligonucleotides used in the present study

Residues in bold indicate restriction enzyme sites, or residues that are mutated.

Name	Sequence (5′→3′)
BamHI-CA1838	GC**GGATCC**CAGGTGCAGCTGCAGG
XhoI-CA1838	GC**CTCGAG**GCTCGACACGGTGACC
S57A	GTGAGGGAGTCGCATCGATT**GCT**AGAGACGGTAATACC
R58	CGTGAGGGAGTCGCATCGATTAGT**GCA**GACGGTAATACCGC
D59A	CTATTAGTAGA**GCC**GGTAATACTGCAGTCTACGCCGACTC
G62A	TAGTAGAGAC**GCT**AATACTGCAGTCTACGCCGACTCCG
N63A	AGAGACGGT**GCT**ACTGCAGTCTACGCCGACTCCGTG
T64A	GTAGAGACGGTAAT**GCT**GCAGTCTACGCCGACTCC
T107A	CTATTACTGGGCC**GCA**TATGTCTTTCCGTGTACC
Y108A	GTGCGGCCACT**GCT**GTCTTTCCGTGCACCAATCCAGG
V109A	GCCACTTAT**GCC**TTTCCGTGCACCAATCCAGGATTC
F110A	CGGCCACTTATGTC**GCT**CCGTGCACCAATCCAGGATTC
T111.2A	CACTTATGTCTTTCCGTGC**GCC**AATCCAGGATTCTCA G
N111.3A	GCCACTTATGTCTTTCCGTGCACC**GCT**CCAGGATTCTCAG
F112.2A	CTTATGTCTTTCCGTGCACCAATCCAGGA**GCC**TCAGAATATCTG
S112.1A	CCAATCCAGGATTC**GCA**GAATATTTGTATAACTACTGGGGCC
E112A	CCAATCCAGGATTCTCA**GCA**TATCTGTATAACTACTGGG
Y113A	CCAGGATTCTCAGAA**GCT**TTGTATAACTACTGGGGCCAGGGG
L114A	GGATTCTCAGAATAT**GCG**TATAACTACTGGGGCCAGGGG

Peptide array synthesis

Fmoc (fluoren-9-ylmethoxycarbonyl) amino acids were activated with HOBt and DIC for 15 min and then spotted on to the membrane using a robotic syringe. To maximize yield, this step was repeated three times for each amino acid. After coupling the Fmoc amino acid, the membrane was removed from the synthesizer and treated with 2 % (v/v) acetic anhydride in DMF to cap any free remaining amino groups. The membrane was then washed with DMF and treated with 20 % (v/v) piperidine in DMF to eliminate the Fmoc group. After washing with DMF and ethanol, the membrane was air-dried and carefully repositioned on the robotic synthesizer for the next coupling cycle. These steps were repeated for each amino acid until the end of the sequence. At the end of this process, all peptides were N-terminally acetylated. The final removal of the side-chain protecting groups was performed by incubating the membrane in a solution of 2 % (v/v) water and 3 % (v/v) TIPS in TFA for 3 h. After extensive washing with DCM, DMF and ethanol, the membrane was air-dried and stored at $-20\,^{\circ}C$ until use.

[1] To whom correspondence should be addressed (email mgalleni@ulg.ac.be).

Figure S1 Alignment of the 56 nanobodies that recognize the VIM-4 MβL

The sequences are arbitrarily grouped according to their CDR3 similarity to reflect the possible differences in their epitope recognition. Residues are numbered according to the IMGT numbering scheme. **, nanobodies that were selected on coated VIM-4. The other nanobodies were obtained through phage display experiments performed in solution.

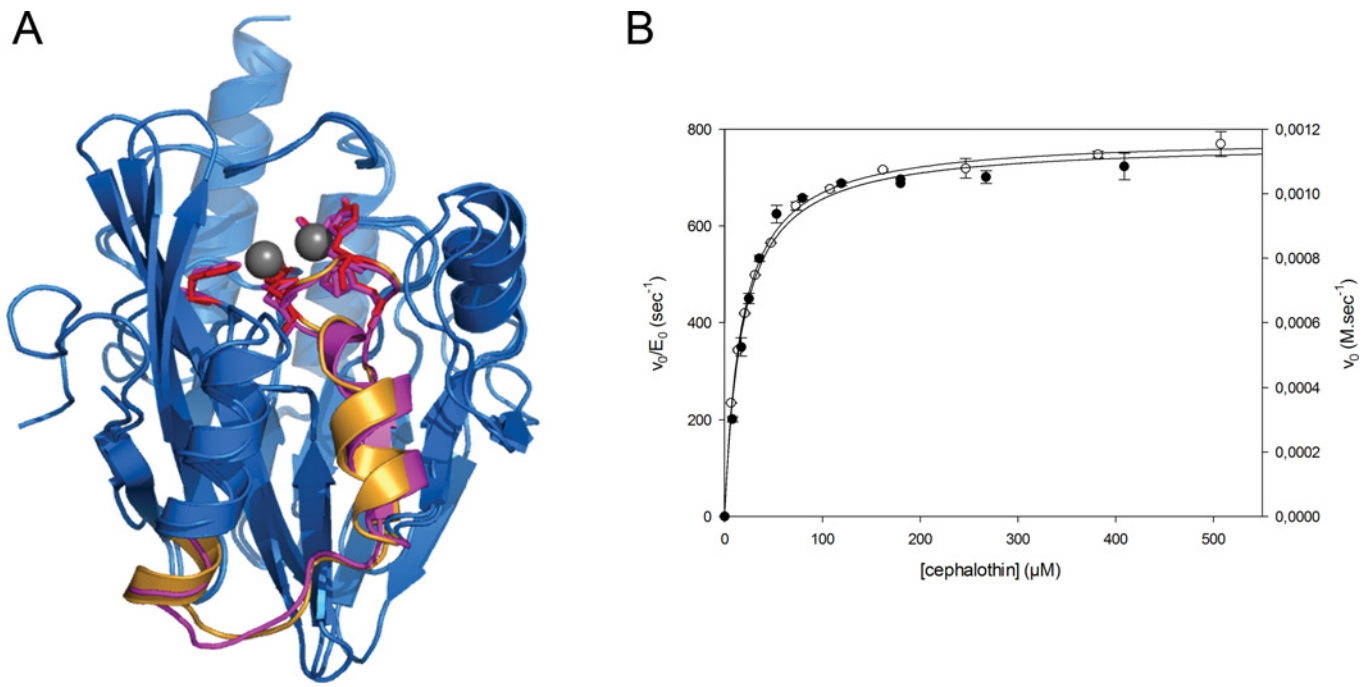

Figure S2 VIMΔepitope

(**A**) Alignment of the crystallographic structures of VIM-4 (PDB code 2WHG) and BlaB (PDB code 1M2X). The epitope region is shown in orange (VIM-4) or magenta (BlaB). (**B**) Michaelis–Menten curves obtained using cephalothin as the substrate. Purified WT VIM-4 (●, left-hand axis). Non-purified hybrid protein VIMΔepitope (○, right-hand axis). The protein VIMΔepitope was designed on the basis of a three-dimensional superimposition of the crystallographic structures of VIM-4 (PDB code 2WHG) and BlaB (PDB code 1M2X). The Michaelis–Menten constant K_m of 17 μM for the hydrolysis of cephalothin by VIMΔepitope was found to be equal to the K_m obtained for WT VIM-4. Thus the chimaeric protein was functional and correctly folded.

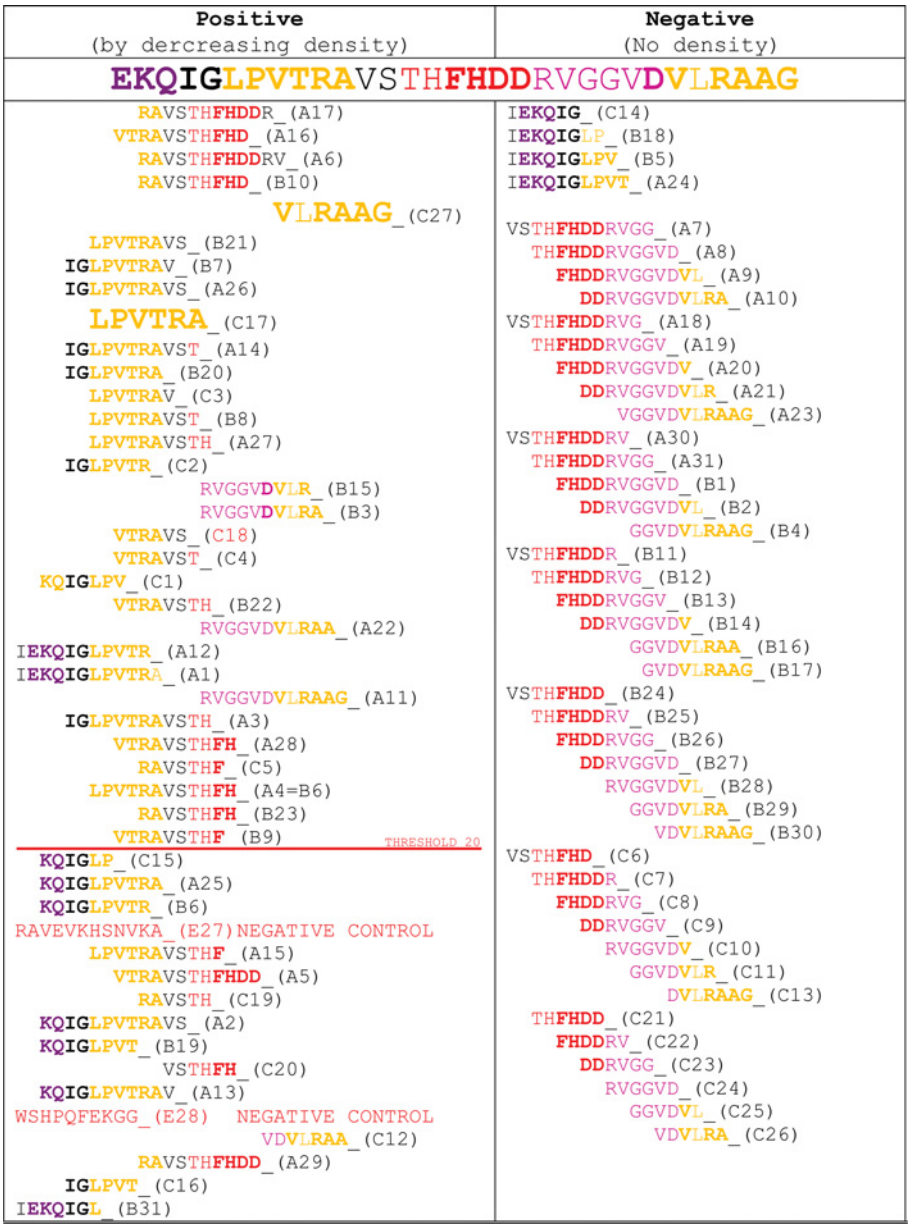

Figure S3 Densitometric analysis of the truncation peptide array

In an attempt to further analyse the Ile^{99}–Gly^{133} epitope, another peptide array experiment was performed using a series of 89 progressively truncated peptides that were spotted and visualized (see the Epitope mapping section in the Experimental section of the main text). After densitometric analysis, the peptides were organized by decreasing densities. In all 99% of the peptides that were devoid of density contained either the entire THFHDDRVGGVD sequence or part of it. This result argues against the presence of the active-site L7 loop at the interface between VIM-4 and cherry–NbVIM_38. However, out of the 31 peptides recognized by cherry–NbVIM_38, 26 contained either the entire LPVTRA motif or a portion of it. More importantly, the two shortest peptides that were clearly recognized were LPVTRA and VLRAAG. In the crystallographic structure of VIM-4, these two peptides coincide with exposed stretches of residues that are in close proximity to each other (L6 loop and the C-terminus of the α2 helix), but distant from the active site. Therefore these two peptides are probably the main binding determinants and constitute the core of this conformational epitope (Figure 5C of the main text).

Received 17 August 2012/11 December 2012; accepted 7 January 2013
Published as BJ Immediate Publication 7 January 2013, doi:10.1042/BJ20121305